FERMILAB-PUB-20-278-E

Charge collection efficiency in back-illuminated Charge-Coupled Devices.

arXiv:2007.04201v1 [physics.ins-det] 8 Jul 2020

Guillermo Fernandez-Moroni[a] **, Kevin Andersson**[a,b] **, Ana Botti**[b] **, Juan Estrada**[a] **, Dario Rodrigues**[a,b] **and Javier Tiffenberg.**[a]

[a] *Fermi National Accelerator Laboratory, PO Box 500, Batavia IL, 60510*
[b] *Department of Physics, FCEN, University of Buenos Aires and IFIBA, CONICET, Buenos Aires, Argentina*

E-mail: gfmoroni@fnal.gov

Abstract: Low noise CCDs fully-depleted up to 675 micrometers have been identified as a unique tool for Dark Matter searches and low energy neutrino physics. The charge collection efficiency (CCE) for these detectors is a critical parameter for the performance of future experiments. We present here a new technique to characterize CCE in back-illuminated CCDs based on soft X-rays. This technique is used to characterize two different detector designs. The results demonstrate the importance of the backside processing for detection near threshold, showing that a recombination layer of a few microns significantly distorts the low energy spectrum. The studies demonstrate that the region of partial charge collection can be reduced to less than 1 μm thickness with adequate backside processing.

Keywords: Back-illuminated CCD, Backside processed CCD, CCE

Contents

1 Thick Fully-Depleted CCDs for Dark Matter and neutrino experiments **1**

2 Determination of the backside CCE using X-rays **2**
- 2.1 Determination of efficiency function using monochromatic X-ray source 3
- 2.2 Determination of efficiency function using an ^{55}Fe source 4

3 Experimental results **5**
- 3.1 Results for CCD-A 6
- 3.2 Results for CCD-B 6
- 3.3 Conclusion 6

1 Thick Fully-Depleted CCDs for Dark Matter and neutrino experiments

Charged Coupled Devices (CCD) with low readout noise and large active volume have been identified among the most promising detector technologies for the low mass direct dark matter search experiments, probing electron and nuclear recoils from sub-GeV DM [1–5]. The recent development of the Skipper-CCD [6, 7] demonstrated the ability to measure ionization events with sub-electron noise extending the reach of this technology to unprecedented low energies. Experiments based on this technology are planned for the coming years with total CCD active mass going from 100 grams to several kilograms [8, 9]. At the same time the low noise CCD technology has been implemented in low energy neutrino experiments [10, 11] and are planned for future developments[12].

There are several key performance parameters for the CCD sensors in future developments that are part of a significant R&D effort for future projects [8, 9, 12]. The most important performance requirements are the pixel dark current [7], readout noise optimization [13], Fano factor [14] and charge transport in the sensor [15].

The Charge Collection Efficiency (CCE) is defined as the fraction of the total charge produced during a ionization event that is collected in the CCD pixel for later readout. For a fully depleted detector, with a large electric field, CCE is approximately 100% [16] for the full active volume. In regions of the detector with lower electric field, CCE could be less than 100% due to charge recombination. Regions of partial CCE distort the measured spectrum of ionization events, affecting energy calibration and particle identification.

Back illuminated CCDs in astronomy are treated to have a thin entrance window for light, with low reflectivity. This is specially important when detectors are used for wavelength shorter than 500 nm [17–19]. A 500 nm photon has an absorption length of 1 μm in Silicon, and any layer with partial charge collection (PCC) on the back surface will degrade the detection efficiency for blue light. The measurements presented in Ref.[20] compare the detection efficiency for visible photons with the reflectivity. These studies show that all photons with wavelength longer than 500 nm are

fully detected, unless they are reflected on the back surface. These results show that the bulk of the detector has 100% CCE, and that any recombination on these sensors occurs only on the first 1μm near the back surface.

For thick CCDs, as those used in dark matter [1–7] and neutrino experiments [10, 11], a backside ohmic contact is required in order to apply the needed substrate bias to fully deplete sensor [21]. At the same time, different processing techniques are used on the backside to reduce dark current. The backside processing of these sensors determines the field shaping near the surface, and has a large impact in the CCE for events in that region. We study here the CCE for back-illuminated detectors with more than 200 μm thickness.

2 Determination of the backside CCE using X-rays

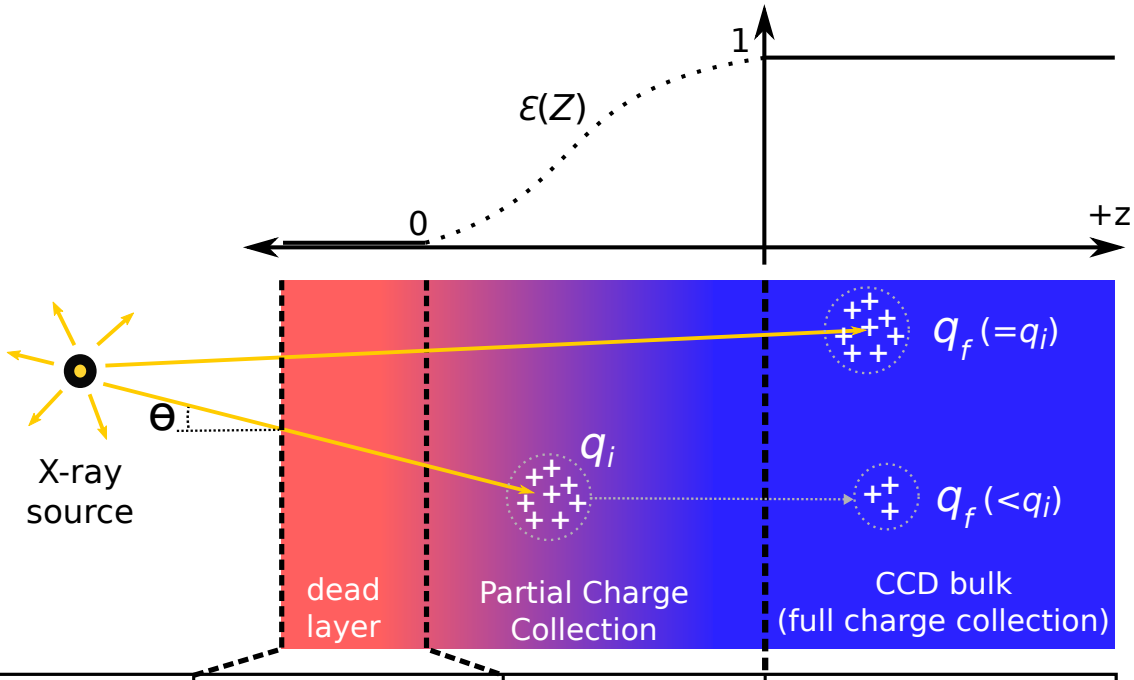

Unthinned CCD-A	2.2µm SiO_2	[0, ?] Si	~670µm Si
Thinned CCD-B	0.1 +0.04+0.02µm SiO_2+ZrO_2+In	[0, ?] Si	~200µm Si

Figure 1. Sketch of the CCD back illumination with an X-ray source. The photon penetrates into the CCD producing a cloud of charge q_i, some fraction $\varepsilon(Z)$ of this charge gets collected depending on the depth Z. The region near the back of the CCD where $0<\varepsilon(Z)<1$ is the PCC layer.

X-rays can be used to characterize the CCE near the back surface of a CCD. Figure 1 shows a cartoon of X-ray setup together with the most important variables that participate in the analysis. Some important aspects and definitions

- The source emits photons with uniform angular distribution covering a full hemisphere. The angular distribution on the sensor depends on the geometry of the setup. We model the angular distribution by $f_\Theta(\theta)$, where Θ is measured as the angle of the incidence of the photon in the CCD compared to perpendicular direction to the back surface of the sensor.

- The X-ray photons can reach the PCC layer and the bulk of the sensor volume. The interaction depth Z in the sensor depends on the incident angle and its probability distribution function (*pdf*) can be written as $f_Z(z|\theta) = (\cos(\theta)/\lambda)\exp(-z\cos(\theta)/\lambda)$, where λ is the attenuation length of the photon.

- X-rays produce an ionization charge packet with mean value $q_i = E_i/\epsilon$, where E_i is the energy of the photon and ϵ= 3.75 eV is the mean ionizing energy [14]. For now, we assume that the initial charge packet is the same for all photoelectric absorption events, we discuss later how the Fano noise affects the final results. The primary charge ionization is the same for the PCC layer and the bulk of the sensor as represented in Fig. 1.

- $\varepsilon(z)$ is the CCE function in the backside of the detector. The function indicates the fraction of carriers that are collected by the pixel after drifting away from the PCC layer (carriers that do not recombine in the PCC layer). This function depends on the depth of the interaction. If the primary charge packet occurs deep in the PCC layer (far from the bulk of the sensor), carrier will have more time to recombine before they reach the bulk. Thus, $\varepsilon(z)$ increases monotonically.

- q_f is the charge that escapes from the PCC layer and can be collected and measured by the sensor. As illustrated in Fig. 1, this will depend on the interaction depth of the photon. We will refer as Q_f to the random variable accounting for the possible values of the X-ray events with *pdf* $f_{Q_f}(q_f)$. The distribution of Q_f is the observable in our data.

From the previous definitions the measured charge can be expressed as

$$Q_f = q_i\varepsilon(Z). \tag{2.1}$$

2.1 Determination of efficiency function using monochromatic X-ray source

The measured spectrum of events normalized by the total number of events (N_T) is an estimation $\hat{f}_{Q_f}(q_f)$ of $f_{Q_f}(q_f)$. We can then use it to estimate the cumulative distribution function (*cdf*) of Q_f:

$$P(Q_f \leq q_f) \approx \hat{F}_{Q_f}(q_f) = \int_0^{q_f} \hat{f}_{Q_f}(x)dx. \tag{2.2}$$

Using Eq.(2.1) and due to the monotonically increasing $\varepsilon(Z)$,

$$P(Q_f \leq q_f) = P(q_i\varepsilon(Z) \leq q_f) = F_Z(z_0) = \int_0^{z_0} \hat{f}_Z(z)dz \tag{2.3}$$

where z_0 is such that $\varepsilon(z_0) = q_f/q_i$, and

$$\hat{F}_{Q_f}(q_f) = F_Z(z_0). \tag{2.4}$$

Table 1. ^{55}Fe X-rays energies, Intensity in photons per 100 disintegrations and attenuation length in μm [22]. Mean e-h pairs production using the mean ionization energy

X_K	Energy (keV)	Mean e-h production (q_i)	Intensity	Attenuation length (λ_α)
α_2	5887.65	1570	8.45 (14)	28.7
α_1	5898.75	1573	16.57 (27)	28.9
β_3	6490.45	1731	3.40 (7)	38.0

.

The measurements at low charge values are often affected by readout noise. In this case, we calculate the *cdf* integrating away from low charge values,

$$\hat{F}^{\leftarrow}_{Q_f}(q_f) = \int_{q_f}^{q_i} \hat{f}_{Q_f}(x)dx, \text{ and } F^{\leftarrow}_{Z}(z_0) = \int_{z_0}^{\infty} \hat{f}_{Z}(z)dz. \tag{2.5}$$

For each q_f, we find z_0 such that $\hat{F}^{\leftarrow}_{Q_f}(q_f) = F^{\leftarrow}_{Z}(z_0)$ where the efficiency is $\varepsilon(z_0) = q_f/q_i$.

The method to calculate the CCE using one X-ray peak is summarized in the Table 2 of the Appendix.

2.2 Determination of efficiency function using an ^{55}Fe source

^{55}Fe X-ray source has an extensive use in the calibration of typical performance parameters of CCDs and other sensors [16]. In this article we extend its use to characterize the charge collection in the PCC layer using the methodology proposed in Section 2.1. The main characteristics of the three X-rays emitted by ^{55}Fe are summarized in Table 1. K_α X-rays have similar energy and attenuation length and therefore can be treated as a single X-ray line for the purpose of this analysis.

Then, *pdf* for the interaction as a function of depth are

$$f_{Z_\alpha}(z|\theta) = (\cos(\theta)/\lambda_\alpha)exp(-z\cos(\theta)/\lambda_\alpha)f_\Theta(\theta)$$

and

$$f_{Z_\beta}(z|\theta) = (\cos(\theta)/\lambda_\beta)exp(-z\cos(\theta)/\lambda_\beta)f_\Theta(\theta)$$

for the X_{K_α} and X_{K_β}, respectively. With the same angular distribution in both cases.

Generalizing Eq. (2.2) and (2.4) for two X-ray energies α and β, the measured *cdf* for Q_f is

$$\hat{F}_{Q_f}(q_f) = P(Q_f \leq q_f) = p_\alpha P(Z_\alpha \leq z_{\alpha,0}) + p_\beta P(Z_\beta \leq z_{\beta,0}), \tag{2.6}$$

where $\varepsilon(z_{\alpha,0}) = q_f/q_{i,\alpha}$ and $\varepsilon(z_{\beta,0}) = q_f/q_{i,\beta}$, such that the depth *cdf* equals the measured cumulative distribution of events. p_α and p_β are the relative intensities determined by Table 1 normalized by the number of desintegrations. Since we assume a monotonically increasing $\varepsilon(z)$ function, then $z_{\alpha,0} \geq z_{\beta,0}$. Using a more condense notation

$$\hat{F}_{Q_f}(q_f) = p_\alpha F_{Z_\alpha}(z_{\alpha,0}) + p_\beta F_{Z_\beta}(z_{\beta,0}) \text{ with } z_{\alpha,0} \geq z_{\beta,0}. \tag{2.7}$$

A recursive nonlinear numeric solver is used to find $z_{\alpha,0}$ and $z_{\beta,0}$ simultaneously. Three features of the ^{55}Fe source can be used to simplify the problem.

- Larger X_{K_α}-flux than X_{K_β}-flux, since $p_\alpha/p_\beta = 7.47$

- $F_{Z_\alpha}(z_{\alpha,0})$ is always greater than $F_{Z_\beta}(z_{\beta,0})$ because of the difference in the attenuation length ($\lambda_\alpha < \lambda_\beta$) and the fact that $z_{\alpha,0} \geq z_{\beta,0}$.

- As q_f becomes smaller than $q_{i,\alpha}$ then $q_f/q_{i,\alpha}$ becomes closer to $q_f/q_{i,\beta}$, and therefore $z_{\alpha,0}$ becomes closer to $z_{\beta,0}$. In fact, $q_{i,\beta}$ and $q_{i,\alpha}$ differ only 10%.

Most of the signal is dominated by the X_{K_α} photon and a small effect is introduced by assuming a unique $z_0 = z_{\alpha,0} = z_{\beta,0}$. This assumption allows to follow the same procedure presented in Section 2.1 to solve equation 2.7. Assuming $z_0 = z_{\alpha,0} = z_{\beta,0}$ the true collection efficiency at z_0 lays between $q_f/q_{i,\beta}$ and $q_f/q_{i,\alpha}$. A simple approximation is $\varepsilon(z_0) = q_f/(p_\alpha q_{i,\alpha} + p_\beta q_{i,\beta})$. The full method for an ^{55}Fe source is summarized in Table 3, in the Appendix.

3 Experimental results

We study here two different CCDs.

CCD-A was designed by the LBNL Microsystems Laboratory [23] as part of the R&D effort for low energy neutrino experiments [10] and low mass direct dark matter search [3]. This is a rectangular CCD with 8 million square pixels of 15 μm × 15 μm each. The CCD is fabricated in n-type substrate with a full thickness of 675 μm. The resistivity of the substrate greater than 10000 Ω-cm. The CCD is operated with 40V bias voltage that fully depletes the high-resistivity substrate using the method developed in Ref.[21]. In order to trap impurities that migrate during the sensor processing, a 1μm thick in-situ doped polysilicon (ISDP) layer is deposited on the backside of the detector. This layer plays a critical role controlling the dark current of the detector. Additional layers of silicon nitride, phosphorous-doped polysilicon and silicon dioxide are added to the backside (2 μm total thickness). Phosphorous can migrate into the high resistivity material producing a region of a few microns where charge can recombine before drifting to the collecting gates of the detector. This region constitutes the PCC layer that we characterize with ^{55}Fe X-rays, as shown in Figure 1.

CCD-B is similar to CCD-A with a few important differences. The detector has 4 million pixels, with a thickness of 200 μm. It is also fabricated in high resistivity n-type silicon. The backside of the sensor has been processed for astronomical imaging. A backside ohmic contact is formed by low-pressure, chemical-vapor deposition in-situ doped polycrystalline silicon (ISDP). This layer is made thin for good blue response, typically 10-20 nm, and is robust to over-depleted operation that is necessary to guarantee full depletion across the entire CCD. This detector is operated at bias voltage of 40 V. Because of its backside treatment, this detector is not expected to have significant charge recombination near the back surface. The detector is exposed to ^{55}Fe X-rays on the backside, as shown in Figure 1.

The ^{55}Fe was located 3.55 cm away from the CCDs. The effective depth distribution of interacting photons was calculated using a Monte Carlo simulation, and the result is

$$f_Z(z) = I_\alpha * exp(-z/\tau_\alpha) + I_\beta * exp(-z/\tau_\beta), \tag{3.1}$$

where $I_\alpha(I_\beta)$ represents the intensity and $\tau_\alpha(\tau_\beta)$ is the effective optical depth for the $\alpha(\beta)$ spectral line. $I_\alpha = 0.034$, $I_\beta = 0.0032$, $\tau_\alpha = 25.74\mu$m, and $\tau_\beta = 37.19\mu$m.

3.1 Results for CCD-A

The spectrum of measured charge for CCD-A is shown in the top panel of Fig. 2, and compared with a Geant4[24] simulation assuming perfect CCE for the entire volume of the sensor ($\varepsilon(z) = 1$). The K_α and K_β peaks from Table 1 are evident. The excess of reconstructed events to the left of these peaks is attributed to the PCC layer, where charge recombination produces a measurement below the peak energy. The bump in the simulation around 1100 e^- is an escape peak, as discussed in Ref.[25]. This data is used to measure the CCE function $\varepsilon(z)$ following the prescription in Section 2.2, and the results are shown in the top panel of Fig.3. The depth scale is chosen such that $\varepsilon(z = 0) = 0.9$. The shaded region corresponds to the energies between 5.4 keV and 7 keV where the events from K_α and K_β are dominant and systematic uncertainties are expected to be important. In this region the precise shape of ε curve is less reliable.

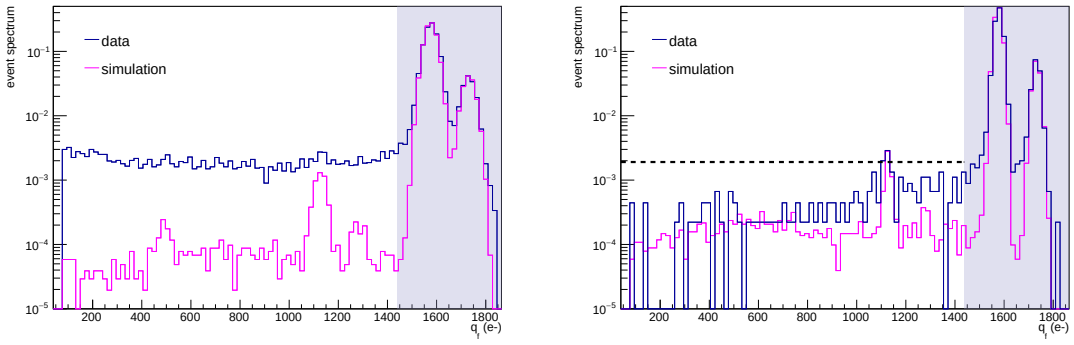

Figure 2. Event spectra for CCD-A (left) and CCD-B (right) calculated using bin size of 70 eV normalized by the number of measured events in the K_α peak. Blue: measured spectra. Magenta: Simulated spectra of events from Geant4. Left figure: spectra for CCD-A; 35195 events in the histogram; 26697 events in the K_α peak. Right figure: event spectra for CCD-B; 5452 events in the histogram; 4482 events in the K_α peak. The dashed black line indicates the expected level of events if the partial charge collection layer on CCD-B was same as the one measured on CCD-A.

3.2 Results for CCD-B

The spectrum of measured charge for CCD-B is shown in the bottom panel of Fig.2, and compared with a Geant4 [24] simulation with perfect CCE. As for CCD-A, the K_α and K_β spectral lines are evident, CCD-B has a different output stage producing higher resolution peaks [6]. The relative rate of events on the left of the peaks, are well below the rate observed for CCD-A and consistent with the simulation. These events are produced mostly by low probability Compton scattering of X-rays. The CCE function $\varepsilon(z_\alpha)$ is determined as discussed in Section 2.2 and the results are shown in Fig.3 bottom panel, black circles. The measurement of $\varepsilon(z_\alpha)$ is also performed after the predicted Compton spectrum is subtracted based on the simulation, the results are shown in bottom panel of Fig.3, magenta circles. As before, the horizontal axis is selected such that $\varepsilon(z = 0) = 0.9$.

3.3 Conclusion

The results of CCD-A and CCD-B showed in Fig.3 demonstrate the large impact that the backside processing could have in the CCE for back-illuminated detectors. When a layer of a few microns with

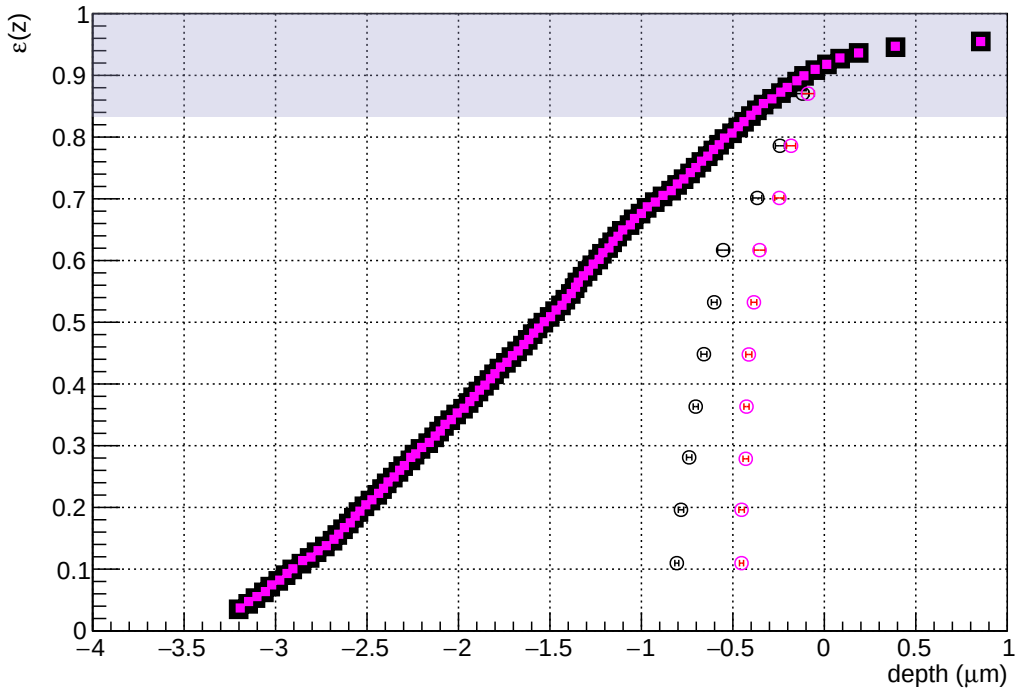

Figure 3. Measured charge collection efficiency for a CCD-A (solid square markers) and CCD-B (open circle markers). The black points show the results without considering the background events predicted by the simulation. The magenta point shows the results after correcting the experimental spectra by subtracting the events form the simulations. The shaded area indicates the region where the detailed shape of the X-ray peaks affect the measurement, introducing more uncertainty.

charge recombination is present on the CCD, the spectrum for low energy X-rays gets significantly distorted. The charge recombination generates a significant number of lower energy events in the spectrum. The backside processing performed in detectors optimized for astronomical instruments eliminates this issue for the most part, as shown with CCD-B. The generation of low energy events constitute a major concern for experiments looking for rare signals near the detector threshold [1–7, 10, 11].

The results obtained here for CCD-B, optimized for astronomical imaging, are consistent with the observations of detection efficiency and reflectivity in Ref.[20].

A new technique was introduced here to characterize the CCE for back-illuminated CCDs, this technique can easily be generalized to other semiconductor detectors. The technique uses tools that are commonly available at the detector characterization laboratories. As shown here, the new method is capable of measuring a PCC layer of a few micrometers. The sensitivity to a very thin PCC layer is limited by the energy of the ^{55}Fe X-rays, and the technique could be easily extended for much thinner recombination layers using lower energy X-rays. This technique will be a powerful tool in the optimization of detectors for the next generation of low threshold experiments looking for rare events such as dark matter, or coherent neutrino nucleus scattering[9, 12].

1) Calculate angular distribution of incident photons:
Based on the geometry of the experiment evaluate $f_\Theta(\theta)$.
2) Calculate depth distribution of events:
$f_Z(z\|\theta) = (\cos(\theta)/\lambda)exp(-z\cos(\theta)/\lambda)f_\Theta(\theta)$, where λ is the attenuation length of the photon. Then, calculate the *cdf* $F_Z(z_0)$ (or $F_Z^{\leftarrow}(z_0)$ from Eq. (2.5)).
3) Make a spectrum of measured events:
Calculate the spectrum of events reconstructed from the data and normalize it by total number of events (N_T). This is the estimation $\hat{f}_{Q_f}(q_f)$.
4) Calculate integral of the measured spectrum up to a charge q_f:
Calculate *cdf* either $\hat{F}_{Q_f}(q_f)$ (from Eq. 2.2), or $\hat{F}^{\leftarrow}_{Q_f}(q_f)$ (from Eq. 2.5).
5) Find z_0:
Find z_0 that equals the *cdf* of the interaction depth with the cumulative proportion of measured events. This is $\hat{F}_{Q_f}(q_f) = F_Z(z_0)$, or $\hat{F}^{\leftarrow}_{Q_f}(q_f) = F_Z^{\leftarrow}(z_0)$.
6) Calculate the efficiency at z_0:
$\varepsilon(z_0) = q_f/q_i$.
7) Repeat steps 4, 5 and 6 for a different q_f to complete $\varepsilon(z)$.

Table 2. Methodology to calculate the PCC efficiency function using one X-ray peak.

Appendix: Details of the method

The details of the method to measure the CCE in the backside of a back-illuminated CCD are presented in Table 2. The details of method used with the ^{55}Fe source having two X-ray lines is presented in Table 3.

Acknowledgments

We thank the SiDet team at Fermilab for the support on the operations of CCDs and Skipper-CCDs, specially Kevin Kuk and Andrew Lathrop. We are grateful to Oscar von Uri for taking care of no-solo-bar problem. This work was supported by Fermilab under DOE Contract No. DE-AC02-07CH11359. This manuscript has been authored by Fermi Research Alliance, LLC under Contract No. DE-AC02-07CH11359 with the U.S. Department of Energy, Office of Science, Office of High Energy Physics. The United States Government retains and the publisher, by accepting the article for publication, acknowledges that the United States Government retains a non-exclusive, paid-up, irrevocable, world-wide license to publish or reproduce the published form of this manuscript, or allow others to do so, for United States Government purposes.

References

[1] A. Aguilar-Arevalo *et al.* (DAMIC), Phys. Rev. **D94**, 082006 (2016), arXiv:1607.07410 [astro-ph.CO]
.

1) Calculate angular distribution of incident photons:
Based on the geometry of the experiment evaluate $f_\Theta(\theta)$.
2) Calculate depth distribution of events:
$f_Z(z\|\theta) = (p_\alpha(\cos(\theta)/\lambda_\alpha)exp(-z\cos(\theta)/\lambda_\alpha) + p_\beta(\cos(\theta)/\lambda_\beta)exp(-z\cos(\theta)/\lambda_\beta))f_\Theta(\theta)$, where λ is the attenuation length of the photon. Then, calculate the cumulative distribution $F_Z(z_0)$ (or $F_Z^{\leftarrow}(z_0)$ from equation 2.5).
3) Make an spectrum of measured events:
Calculate the spectrum of events reconstructed from the data and normalize it by total number of events (N_T). This is the estimation $\hat{f}_{Q_f}(q_f)$.
4) Calculate integral of the measured spectrum up to a charge q_f:
Calculate cumulative distributions either $\hat{F}_{Q_f}(q_f)$ (from Eq. 2.2), or $\hat{F}^{\leftarrow}_{Q_f}(q_f)$ (from Eq. 2.5).
5) Find z_0:
Find z_0 that equals the *cdf* of the interaction depth with the cumulative proportion of measured events. This is $\hat{F}_{Q_f}(q_f) = F_Z(z_0)$, or $\hat{F}^{\leftarrow}_{Q_f}(q_f) = F_Z^{\leftarrow}(z_0)$.
6) Calculate the efficiency at z_0:
$\varepsilon(z_0) = q_f/(p_\alpha q_{i,\alpha} + p_\beta q_{i,\beta})$
7) Repeat steps 4, 5 and 6 for a different q_f to complete $\varepsilon(z)$.

Table 3. Methodology to calculate the partial charge collection efficiency function using ^{55}Fe source.

[2] A. Aguilar-Arevalo *et al.* (DAMIC), Phys. Rev. Lett. **118**, 141803 (2017), arXiv:1611.03066 [astro-ph.CO] .

[3] A. Aguilar-Arevalo *et al.* (DAMIC), Phys. Rev. Lett. **123**, 181802 (2019), arXiv:1907.12628 [astro-ph.CO] .

[4] M. Crisler, R. Essig, J. Estrada, G. Fernandez, J. Tiffenberg, M. Sofo haro, T. Volansky, and T.-T. Yu (SENSEI), Phys. Rev. Lett. **121**, 061803 (2018), arXiv:1804.00088 [hep-ex] .

[5] O. Abramoff *et al.* (SENSEI), Phys. Rev. Lett. **122**, 161801 (2019), arXiv:1901.10478 [hep-ex] .

[6] J. Tiffenberg, M. Sofo-Haro, A. Drlica-Wagner, R. Essig, Y. Guardincerri, S. Holland, T. Volansky, and T.-T. Yu, Phys. Rev. Lett. **119**, 131802 (2017), arXiv:1706.00028 [physics.ins-det] .

[7] L. Barak, I. M. Bloch, M. Cababie, G. Cancelo, L. Chaplinsky, F. Chierchie, M. Crisler, A. Drlica-Wagner, R. Essig, J. Estrada, E. Etzion, G. Fernandez Moroni, D. Gift, S. Munagavalasa, A. Orly, D. Rodrigues, A. Singal, M. Sofo Haro, L. Stefanazzi, J. Tiffenberg, S. Uemura, T. Volansky, and T.-T. Yu, arXiv e-prints , arXiv:2004.11378 (2020), arXiv:2004.11378 [astro-ph.CO] .

[8] M. Settimo, arXiv e-prints , arXiv:2003.09497 (2020), arXiv:2003.09497 [hep-ex] .

[9] The Oscura project is an R&D effort supported by Department of Energy to develop 10 kg skipper-CCD dark matter search.

[10] A. Aguilar-Arevalo *et al.* (CONNIE Collaboration), Phys. Rev. D **100**, 092005 (2019).

[11] Connie Collaboration, A. Aguilar-Arevalo, X. Bertou, C. Bonifazi, G. Cancelo, B. A. Cervantes-Vergara, C. Chavez, J. C. D'Olivo, J. C. Dos Anjos, J. Estrada, A. R. Fernandes Neto, G. Fernandez-Moroni, A. Foguel, R. Ford, F. Izraelevitch, B. Kilminster, H. P. Lima, M. Makler,

J. Molina, P. Mota, I. Nasteva, E. Paolini, C. Romero, Y. Sarkis, M. S. Haro, J. Tiffenberg, and C. Torres, Journal of High Energy Physics **2020**, 54 (2020), arXiv:1910.04951 [hep-ex] .

[12] The Violeta Collaboration is planning a kg-scale Skipper-CCD experiment at a nuclear reactor facility.

[13] G. Cancelo, C. Chavez, F. Chierchie, J. Estrada, G. Fernandez Moroni, E. E. Paolini, M. Sofo Haro, A. Soto, L. Stefanazzi, J. Tiffenberg, K. Treptow, N. Wilcer, and T. Zmuda, arXiv e-prints , arXiv:2004.07599 (2020), arXiv:2004.07599 [astro-ph.IM] .

[14] D. Rodrigues *et al.*, (2020), arXiv:2004.11499 [physics.ins-det] .

[15] M. Sofo Haro, G. Fernandez Moroni, and J. Tiffenberg, arXiv e-prints , arXiv:1906.11379 (2019), arXiv:1906.11379 [physics.ins-det] .

[16] J. R. Janesick, *Scientific charge-coupled devices*, Vol. 83 (SPIE press, 2001).

[17] S. Nikzad, M. E. Hoenk, P. J. Grunthaner, R. W. Terhune, F. J. Grunthaner, R. Winzenread, M. M. Fattahi, H.-F. Tseng, and M. P. Lesser, in *Proceedings of the SPIE*, Society of Photo-Optical Instrumentation Engineers (SPIE) Conference Series, Vol. 2198, edited by D. L. Crawford and E. R. Craine (1994) pp. 907–915.

[18] E. T. Hamden, A. D. Jewell, C. A. Shapiro, S. R. Cheng, T. M. Goodsall, J. Hennessy, M. Hoenk, T. Jones, S. Gordon, H. R. Ong, D. Schiminovich, D. C. Martin, and S. Nikzad, Journal of Astronomical Telescopes, Instruments, and Systems **2**, 036003 (2016), arXiv:1701.02733 [astro-ph.IM] .

[19] C. J. Bebek, J. H. Emes, D. E. Groom, S. Haque, S. E. Holland, P. N. Jelinsky, A. Karcher, W. F. Kolbe, J. S. Lee, N. P. Palaio, D. J. Schlegel, G. Wang, R. Groulx, R. Frost, J. Estrada, and M. Bonati, Journal of Instrumentation **12**, C04018 (2017).

[20] M. H. Fabricius, C. J. Bebek, D. E. Groom, A. Karcher, and N. A. Roe, in *Proceedings of the SPIE*, Society of Photo-Optical Instrumentation Engineers (SPIE) Conference Series, Vol. 6068, edited by M. M. Blouke (2006) pp. 144–154.

[21] S. E. Holland, D. E. Groom, N. P. Palaio, R. J. Stover, and M. Wei, IEEE Transactions on Electron Devices **50**, 225 (2003).

[22] M.-M. Bé, V. Chisté, C. Dulieu, E. Browne, C. Baglin, V. Chechev, N. Kuzmenko, R. Helmer, F. Kondev, D. MacMahon, and K. Lee, *Table of Radionuclides*, Monographie BIPM-5, Vol. 3 (Bureau International des Poids et Mesures, Pavillon de Breteuil, F-92310 Sèvres, France, 2006).

[23] Https://engineering.lbl.gov/microsystems-laboratory/.

[24] Https://geant4.web.cern.ch.

[25] J. Jaeckel and S. Roy, Phys. Rev. **D82**, 125020 (2010), arXiv:1008.3536 [hep-ph] .